Long working distance high resolution reflective sample imaging via structured embedded speckle illumination

Aswin Haridas,[1,2, ‡] Sandeep Menon Perinchery,[1,2, ‡] Anant Shinde,[2] Oleksandr Buchnev,[3] and Vadakke Matham Murukeshan[1,2*]

[1]*School of Mechanical and Aerospace Engineering, Nanyang Technological University, Singapore 639798.*
[2]*Centre for Optical and Laser Engineering, 50 Nanyang Avenue, Singapore 639798.*
[3]*Optoelectronics Research Centre, University of Southampton, Building 53 University road, Highfield Southampton S017 1BJ.*
‡Equal Contribution

A R T I C L E I N F O

Keywords:
High-resolution imaging
Long working distance imaging
High SNR imaging
Optical microscopic imaging
Structured illumination
Embedded speckle patterns

A B S T R A C T

Imaging beyond the diffraction limit at longer working distances using enhanced microscopic configurations has always been a challenge for biological and engineering samples. Even though multiple techniques have been widely used for sub-diffraction limit resolution imaging, the achievable resolution was relying on the use of objective lenses with a high numerical aperture (NA). In the case of engineering samples, in addition to sustaining higher resolutions at large working distances, improving the signal-to-noise ratio (SNR) is also critical. In this context, we propose and demonstrate a concept for high-resolution imaging at large working distances, termed as structured illumination embedded speckle microscopy. An imaging resolution of ~ 310 ± 5 nm was achieved with a microscope objective (0.55 NA; 50X) having 11 mm long working distance using a Siemen's star as the test sample. The demonstrated microscopy is therefore envisaged for engineering applications that demands high-resolution, high SNR imaging at long working distances.

1. Introduction

Over the past few decades, numerous far-field optical imaging techniques have been developed for high resolution imaging of biological and engineering samples. Techniques including confocal microscopy [1-9], structured illumination microscopy (SIM) [10-13], stimulated emission depletion microscopy (STED) [14], stochastic optical reconstruction microscopy (STORM) [15] photoactivated localization microscopy (PALM) [16] and superoscillation imaging [17-20] have transformed high resolution imaging in biological and engineering applications. Among these techniques, all of which enhance the optical transfer function (OTF) support of conventional microscopy, confocal microscopy is probably the most attractive and widely used due to its ability to produce high-resolution, optically sectioned images. Even though multiple adaptation of confocal microscopes exists, the scanning confocal microscopy [9] and spinning Nipkow disk confocal microscopy [6] has gained wide popularity. However, scanning large fields of view using a scanning confocal microscope and a poor light efficiency of the Nipkow disk have limited its use. An alternate technique for optical sectioning and high-resolution imaging is structured illumination microscopy (SIM). Lately, apart from high resolution imaging of biological samples, several authors have discussed the implementation of SIM for high resolution surface topography measurements of critical micro optical components. In optical metrology, SIM is a highly accurate, incoherent (low noise) method that characterizes the microtopography of rough and smooth surfaces with high resolutions [21-27]. In principle, for surface measurements, a sinusoidal fringe pattern is projected onto the object surface through a microscopic objective. The modulated fringe pattern upon reflection from the sample is then imaged onto the detector through the same microscopic objective for 3D profile extraction.

The resulting surface topography estimated using SIM was found to be comparable to high resolution images obtained from a scanning tunneling microscope (SEM) [21]. In all these cases, in order to attain sub-diffraction limit resolutions, objective lenses of high numerical apertures (NA) were used. However, high NA objectives have very small working distances between the lens plane and the object plane resulting in possible sample contaminations and undesirable contact on the sample surface. This is of concern especially for imaging biological specimen and engineered surfaces with high slopes.

More recently, for high-resolution imaging and optical sectioning in fluorescence microscopy, the use of speckle pattern illumination instead of periodic grating illumination (used for SIM) was suggested [28-33]. To date, several techniques have been proposed to perform high-resolution imaging, which may be separated into three basic categories. In the first category, super resolution imaging is achieved by combining optical processing techniques followed by digital restoration [28-33]. In the optical processing phase, a speckle-encoded input is generated by imaging a series of time variant, random or correlated speckle patterns projected onto the sample via a low NA objective lens. Further, the digital restoration phase decodes the super resolution image from the captured series using an image captured with a known a-priori speckle pattern projected onto the sample via a high NA objective lens [33]. Alternatively, the second category of techniques for super-resolution fluorescence imaging exploits the statistical properties of the speckle pattern illumination which controls the temporal emission fluctuations of the fluorophores [34-36]. Using this technique for fluorescent microscopy, resolution enhancements of up to 1.6 times has been reported [32]. However, the cumbersome processing required to estimate the illumination patterns to generate the super resolution image limits the time efficiency of the technique. The third strategy employs a differential intensity variance algorithm between consecutive images captured with dynamic speckle pattern illumination. Background noise reduction and depth discrimination has been observed to be on par with confocal microscopy [37-43].

Here, we propose a long working distance microscopic system for high resolution imaging of engineered surfaces using structured illumination embedded speckle microscopy. We investigate the synergy

* Corresponding author. Tel./fax: (+65) 6790 4200,
E-mail address: mmurukeshan@ntu.edu.sg (V.M. Murukeshan)

resulting from the combination of SIM and speckle pattern illumination, since the imaging resolution improvement using the latter is inferior to the former [10, 32]. Static and dynamic speckle patterns are embedded within the conventional periodic illumination patterns to enhance imaging resolutions. An illustrative imaging analysis confirming far-field sub-diffraction limit resolution at longer working distances is carried out using a reflective Siemen's star as the test sample. Spatial features resolvable by a longer working distance objective (50X; 0.55 NA) using a conventional microscope and the proposed system are compared. Apart from lateral resolution comparisons, the mean square error (MSE) and signal-to-noise ratio (SNR) are calculated to study artefacts reduction using the proposed configuration. The proposed technique is envisaged for high-resolution, high SNR imaging for various engineering applications.

2. Materials and Method

2.1 Structured illumination embedded speckle microscope: Optical Configuration

The schematic diagram of structured illumination embedded speckle microscope is shown in Figure 1. A 561 nm diode laser serve as the excitation source (Coherent Inc, OBIS laser box, USA). A 50X Nikon TU Plan ELWD corrected long working distance microscope objective (50X, NA 0.55, 11 mm working distance) is used as the objective lens. The laser light scattered from a diffuser is expanded and modulated by a reflective phase-only spatial light modulator (LCOS-SLM; HOLOEYE, LETO). The modulated light is passed through a polarizer and focused by a plano-convex lens (LA-1979-A, Thorlabs, F= 200 mm) on to the back aperture of the microscopic objective lens. The light from the microscope objective lens was then collected through a tube lens (ITL 200, Thorlabs). Finally, the images of the sample surface were captured using an EMCCD camera (iXON 887 Andor, Canada). A LABVIEW© interface was incorporated to automate pattern projection and image acquisition. The phase-only reflective SLM, 3-axis stage and the camera were programmed to execute a sequential function. For measurements performed using the conventional SIM arrangement, the diffuser in the illumination arm was removed.

For structured illumination embedded speckle microscopy, static and dynamic speckle patterns are embedded within the conventional SIM gratings. While, static speckles are generated using a ground glass diffuser, DG10-1500-MD (THORLABS©), dynamic speckle patterns are generated using electroactive optical diffusers, LSR-C-3005-1 and LSR-C-3005-6D-VIS (Optotune). Conventional microscopy measurements are performed by setting the LCOS-SLM in the switch off mode. Although, the proposed microscope necessitates additional components to be introduced within the illumination arm of a conventional microscope, the optical configuration can be optimized to ensure there are only a little or no moving parts (e.g. using the electroactive optical diffuser), minimizing the errors resulting from optical alignment issues. In addition, since the laser light in the modified scheme is used to generate the speckle patterns, the laser power has to be carefully selected to ensure a bight illumination, within the selected Field-of-View (FOV).

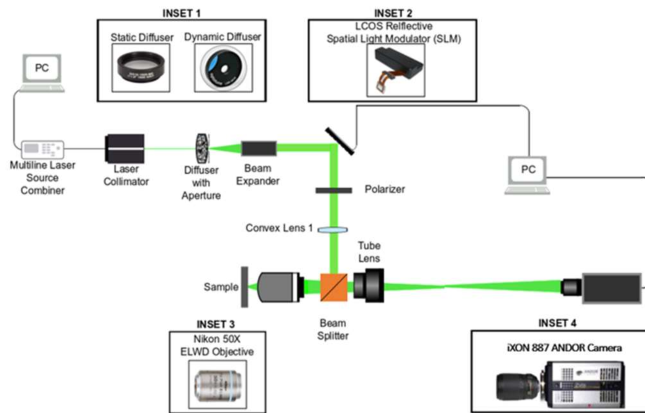

Fig. 1. Schematic diagram for embedding speckle patterns within structured illumination used for a conventional structured illumination microscope (SIM).

2.2 Illumination patterns and image processing

Several implementations of structured illumination microscopy have been reported in literature [2, 10-14, 21-27]. Super resolution SIM (SR-SIM) is one of the widely used and accepted techniques for imaging biological samples at sub-diffraction limit resolutions. The technique has been known to achieve a two-fold improvement in lateral resolutions for fluorescent based bioimaging [10]. Lateral resolution improvements using SR-SIM can be credited to the moiré effect. The resultant emission distribution when a sample is illuminated by a series of structured illumination patterns forms moiré fringes. These fringes can be used to determine the finer structures on the sample if the orientation and position of the structured illumination patterns are known. On the other hand, for high-resolution imaging of reflected samples. Optical sectioning SIM (OS-SIM) has been widely used [21-27]. The principle of OS-SIM is to enhance the in-focus information from the sample and eliminate the out-of-focus information. Unlike SR-SIM, OS-SIM offers advantages that includes ease of implementation and reduced data processing requirements making it a suitable candidate for industrial applications that require high-resolution imaging capabilities. Considering the aforementioned advantages, here we have used the OS-SIM algorithm for high-resolution imaging of engineering samples.

For imaging using a conventional OS-SIM configuration, a reflective phase-only spatial light modulator (SLM; HOLOEYE, LETO) is used to generate the illumination patterns. With a pixel pitch of 6.4 μm and an interpixel gap of 0.2 μm, the LETO reflective LCOS micro display has a resolution of 1920 X 1080-pixels (full HD). This LCOS-SLM can modulate the grayscale level of any pixel between 0 and 255 with a switching rate of 60 Hz. For conventional SIM, three images (with a 1200 phase difference between each image) are captured by the EMCCD camera. This is repeated for two illumination pattern orientations, each rotated by 120º and 240º, respectively. Figure 2, shows the nine patterns loaded onto the LCOS-SLM to generate the illumination patterns.

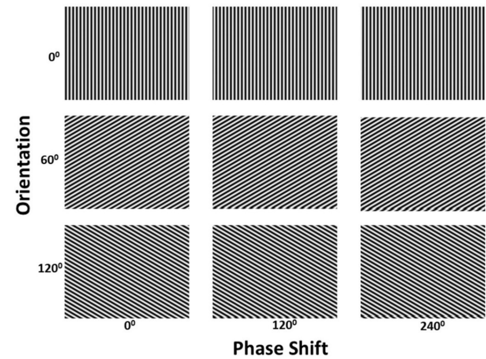

Fig. 2. Periodic illumination patterns projected onto the LCOS reflective phase-only SLM to modulate the illumination.

The resultant image is calculated using the relation [22],

$$I_p = \left[(I_1 - I_2)^2 + (I_2 - I_3)^2 + (I_1 - I_3)^2 \right]^{1/2} \quad (1)$$

Here, I_1, I_2 and I_3 are the three images captured using the illumination patterns phase shifted by 0º, 120º and 240º respectively. I_p is the resultant image determined from the three phase shifted images.

For structured illumination embedded speckle microscope, the conventional SIM images are modified by embedding speckle patterns within the periodic gratings. In this study, to determine the influence of physical properties of the speckle pattern on the performance of the proposed microscope, two different schemes are employed for speckle pattern generation,

a) Static speckles generated using a ground glass diffuser, DG10-1500-MD (THORLABS©) – and,
b) Dynamic speckle patterns generated using two electroactive optical diffusers

The relevance of speckle patterns generated using these techniques arises from the possibilities of modifying the average speckle size (smallest – largest) and varying the projection frame rate (number of speckle patterns projected in relation to the frame rate of the camera).

Static speckles generated using a ground glass diffuser, DG10-1500-MD (THORLABS©) are used for structured embedded static speckle illumination microscopy. Additionally, an aperture placed adjacent to the diffuser was used to control the speckle size. Figure 3 (a), shows the modified illumination patterns used for structured illumination embedded speckle microscopy. Here, we have used a laser illumination source to have an effective control over the projected speckle patterns. For the proposed configuration, several statistically independent speckle patterns generated by rotating the ground glass diffuser are embedded within the grating patterns. This ensures that the entire sample is illuminated. For every speckle pattern embedded within the periodic illumination, the resultant intermediate image is calculated using equation 1. The final image is then calculated by averaging the intermediate resultant images. In order to study the effect of speckle size, speckle patterns with varying sizes are embedded within the grating structure as shown in Figure 3 (b).

For structured embedded dynamic speckle illumination microscopy, dynamic speckle patterns are generated using two electroactive optical diffusers. These are nothing but moving diffusers (oscillation frequency of 300 Hz; oscillation amplitude of 300 μm; in comparison, EMCCD maximum full-frame rate is 25 fps). An electroactive optic diffuser constitutes of an elastic membrane surrounded by electrodes. When actuated, these electrodes induce circular oscillations to the elastic membrane. Two optical diffusers, D_1 - LSR-C-3005-1 and D_2 - LSR-C-3005-6D-VIS are used for this study. Having a particle density of 13 (#/mm^2) and a particle size of 100 μm, the diffusion angle of D_1 is 1^0. On the other hand, having a diffusion angle of 6^0, D_2 has a much larger particle density (42 (#/mm2)) consisting of smaller particles (30 μm). These temporally varying uncorrelated speckle patterns were embedded within the SIM gratings. Example of an illumination pattern used for this configuration is shown in Figure 4. The temporal variation of intensity due to the oscillations of the electroactive optic diffusers are shown in the inset. The process flowchart for the high-resolution microscope is described in *Appendix A* (Figure 14).

In comparison to the algorithm proposed here to determine the high-resolution images, those reported in the literature requires several additional iterative steps to determine a high-resolution image from a series of images obtained by projecting speckle patterns onto the sample surface. Since most of the reported techniques are meant for fluorescence imaging, the algorithms take advantage of (and their accuracies are dependent on) the statistical properties of the projected speckle patterns (speckle contrast or speckle correlation). Since the proposed technique is independent of the statistical properties of the speckle pattern, the overall processing time is reduced. Furthermore, by implementing dynamic speckle patterns using an electroactive optical diffuser and an SLM, the switching speed (time taken between two speckle pattern projections) can be minimized, which therefore reduces the overall measurement time (including the time taken for processing the images).

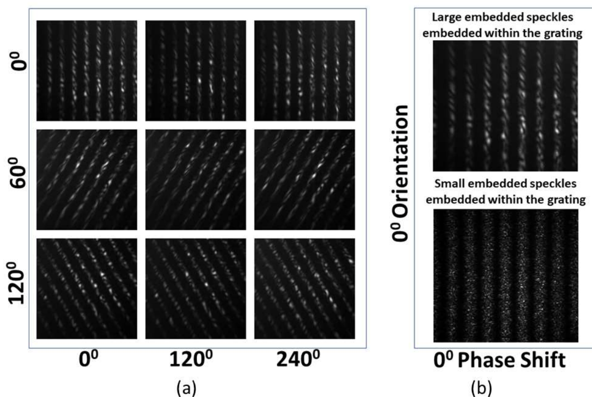

Fig. 3. (a) Modified SIM patterns incorporating speckle patterns, (b) different speckle sizes used for modulating the illumination grid having a 0^0-orientation phase shifted by 0^0. The speckle size variations are achieved by changing the size of the aperture placed after the diffuser.

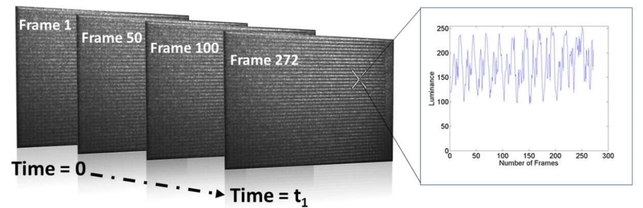

Fig. 4. Shows the patterns modified using dynamic speckle patterns generated using an electroactive optic diffuser from Optotune (LSR-3005-6D-VIS). Additionally, the temporal luminance variation (time, T = 0 to T = t_1) incorporating a dynamic speckle is shown in the inset.

2.3 Structured illumination embedded speckle Microscopy: Working Principle

The principle of structured illumination embedded speckle microscopy is depicted in Figure 5.

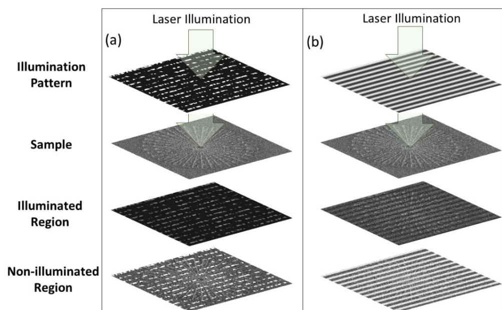

Fig. 5. The working principle of (a) structured illumination embedded speckle microscope and (b) SIM.

When a reflective sample is illuminated using structured embedded speckle illumination the scattering noise suppression via structured illumination is enhanced by the speckle pattern illumination having spots with random shapes illuminating smaller sample areas. Figure 5 (a) shows the illuminated and non-illuminated regions imaged via structured embedded speckle illumination using Siemen's star as the test sample. Figure 5 (b), shows the same sample illuminated by structured illumination. By observing the illuminated and non-illuminated regions on the sample as a result of each of these illumination schemes, reduced scattering and therefore enhanced imaging quality can be predicted for the proposed configuration.

Since the image quality is predicted to be dependent on the size of the illuminated region (controlled in this case by the size of the grating pattern and the average speckle size), the structured embedded dynamic speckle illumination microscopy is expected to outperform the structured embedded static speckle illumination microscopy. This is because, the particle densities and particle sizes of the electroactive optical diffusers are much smaller than the ground glass diffusers that are used to generate the static speckle patterns. Furthermore, since the performance of the proposed optical arrangement is dependent on the total number of the projected speckles used, the latter is also expected to reduce the overall measurement time (due to a faster switching rate), whilst maximizing the performance.

2.4 Image Quality Assessment

In order to assess the image quality, two error metrics, namely, the mean square error (MSE) and peak signal-to-noise ratio (PSNR) are used. The MSE represents the cumulative squared error between the two images, whereas PSNR is a measure of the peak error between the two images. Typically, the error metrics are determined to compare the quality of a compressed image to a reference image, commonly known as the ground truth image [45]. In this study, we compare the images captured using the conventional SIM and structured illumination embedded speckle microscope to a ground truth image.

To compute the MSE, the following mathematical equation is used [46],

$$MSE = \frac{\sum_{M,N} [I_1(m,n) - I_2(m,n)]^2}{M \times N} \quad (2)$$

Here, M and N are the number of rows and columns in the image, I_1 *(m, n)* and I_2 *(m, n)* are the intensity values of the mth and nth pixel, respectively. The calculated MSE value is used to evaluate the PSNR using the relation [46],

$$PSNR = 10 \log_{10}\left(\frac{R^2}{MSE}\right) \quad (3)$$

Where, R is the maximum fluctuation in the input image data type.

3. Results and Discussions

3.1 Conventional Microscope and Structured Illumination Imaging using a Siemen's star as the test sample

A Siemen's star which is used as the test sample is imaged using a scanning electron microscope (SEM) and our system in the conventional microscope configuration (using a 50X; 0.55 NA microscopic objective; Illumination laser source used was a 561 nm Gaussian beam). The images obtained are shown in Figures 6 (a) and (b), respectively. The inset in the figure 6 (b) shows a quadrant of the Siemen's star which has been cropped and enlarged. The inset clearly shows a deteriorated image resolution and image contrast which could possibly be prominently due to scattering noise as a result of illuminating the entire sample area. In addition to the dominant scattering noise, issues including (but not limited to) interference of the speckle patterns and the quality of the optical components could also have presumably contributed to the deteriorated image resolution and image contrast.

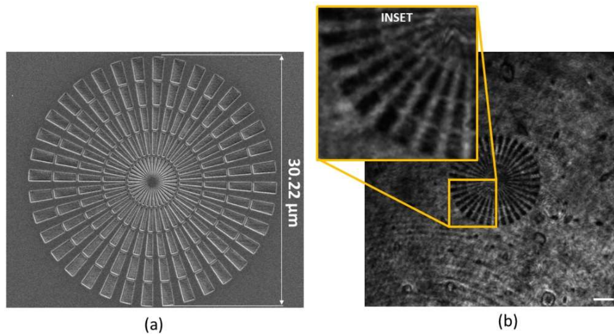

Fig. 6. Images obtained from a conventional SEM and a conventional microscope using a Siemen's star as the test sample. The white scale bar indicates 7.5 µm.

The images obtained from our system in the SIM configuration using a Siemen's star test chart is shown in Figure 7.

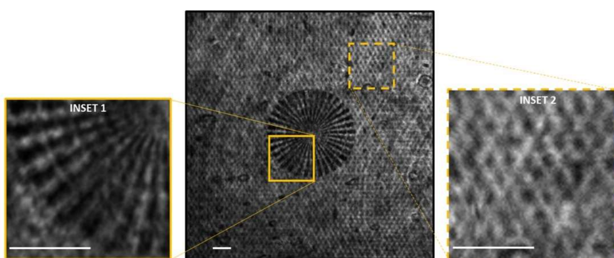

Fig. 7. Images obtained from our system in the SIM configuration using a Siemen's star as the test sample. Insets 1 and 2 represents the resolvable Siemen's star spokes and the artefacts errors due to the sectioning SIM algorithm, respectively. The white scale bar in each image indicate 7.5 µm.

The expanded 561 nm Gaussian laser beam is modulated by a reflective phase-only spatial light modulator (SLM; HOLOEYE, LETO) in the illumination arm of the microscope. Periodic grating patterns illuminate the sample through a microscopic objective lens. Optical sectioning and image reconstruction algorithms are applied onto the captured images (for details, see section *2.2*). Even though SIM reduces the scattering noise considerably, the presence of grid pattern noise (resulting from phase/rotation errors of the grid pattern) is observed to affect the imaging resolutions (see Insets 1 and 2 in Figure 7) [33].

3.2 Structured embedded static speckle illumination microscopy using a Siemen's star as the test sample

Figure 8, shows the images obtained from the structured embedded static speckle illumination microscope using the Siemen's star as the test sample. Each of the images shown in Figure 8 is generated using five statistically independent speckle patterns embedded within the periodic gratings. Fig 8 (a) and Fig 8 (b), shows the images obtained from structured embedded static speckle illumination microscopy with varying speckle sized using Siemen's star as the test sample. It has to be noted that similar camera parameters (such as the integrating time and the frame rate) were used for all tests.

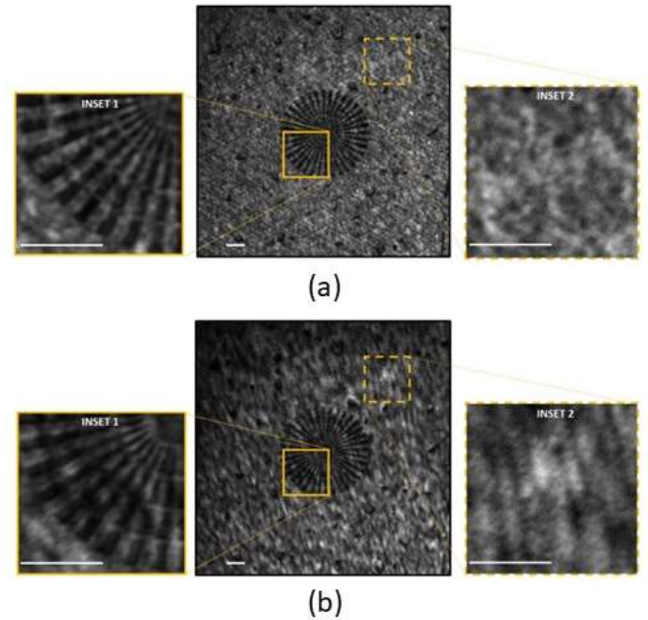

Fig. 8. (a) and (b) shows the images obtained from the structured illumination embedded speckle microscope using a Siemen's star test chart for varying speckle sizes. The speckle size used for (a) is comparatively smaller than (b). The insets 1 and 2 of (a) and (b) shows the image quality achieved and the reduction in artefact errors, respectively. The white scale bar in each image indicate 7.5 µm.

Apart from the attenuated grid pattern noise, the imaging resolution and the brightness are found to be improved in comparison with Figures 6 (b) and 7. Additionally, structured illumination embedded speckle microscope using smaller speckle patterns is observed to effectively subdue the scattering noise as compared to using larger speckle patterns. This could be associated to the smaller illumination spot size offered by the latter that results in the illumination of smaller sample areas.

3.3 Structured embedded dynamic speckle illumination microscopy using a Siemen's star as the test sample

Figure 9, shows the Siemen's star imaged using structured embedded dynamic speckle illumination microscopy. In comparison with the conventional imaging system, the improvement in resolution is significant. This is evident when comparing Figures 9 (a) and (b) with Figures 6 (b) and 7. Even though the imaging contrast and brightness has improved, the grid pattern noise due to the periodic illumination patterns are retained. Nevertheless, compared with conventional SIM, the grid noise is clearly subdued (See inset 2 in Figure 7, Figure 9 (a) and Figure 9 (b)).

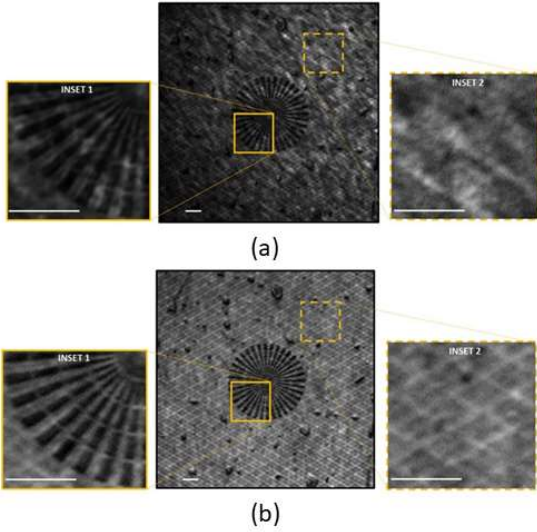

Fig. 9. Shows the images obtained from the structured embedded dynamic speckle illumination microscopy using a Siemen's star as the test sample with dynamic speckle patterns generated using (a) LSR-C-3005-1 and (b) LSR-C-3005-6D-VIS. Insets 1 and 2 represents the resolvable Siemen's star spokes and the reduced artefacts errors, respectively. The white scale bar in each image indicate 7.5 µm.

3.4 *Spatial Resolution of the structured illumination embedded speckle microscope*

Figures 10 (a), (b) and (c) show the comparison of circular image profiles using a Siemen's star as the test sample obtained from the conventional SIM and the structure embedded static and dynamic speckle illumination microscope, respectively.

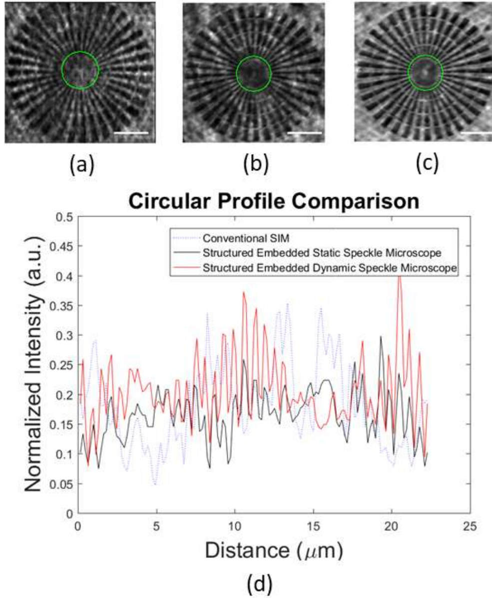

Fig. 10. Images obtained from the conventional SIM (a) is compared with structured embedded (b) static and (c) dynamic speckle illumination microscopy using Siemen's star as the test sample. The comparison of circular section profiles of the Siemen's star test chart indicated by the green circles in (a), (b) and (c) is shown in (d). The white scale bar in each image indicate 7.5 µm.

Notably, the image resolution and image contrast of structured illumination embedded speckle microscope is superior to the conventional SIM. The graph plotted in Fig 10 (d) establishes the improved imaging resolution of the proposed microscope. Figures 15 and 16 (in *Appendix B*) show the comparison of circular image profiles obtained using a SEM, conventional microscopy and SIM.

In order to evaluate the spatial resolution of the structured illumination embedded speckle microscope, we compare the measured resolutions with the theoretical resolution limit [9,10].

The Rayleigh's resolution limit for the 50X microscope objective with 0.55 NA is calculated using equation (4) as, 622.2 nm.

$$\text{Rayleigh Resolution} = \frac{0.61 \times \lambda}{NA} \tag{4}$$

Here, λ is the wavelength of light (561 nm) and NA is the Numerical Aperture of the objective lens used. A comparison of the lateral resolutions obtained via conventional microscopic configurations and the structured illumination embedded speckle microscopy using Siemen's star as the test sample is shown in Figure 11.

From Figures 11 (a) – (f), it can be observed that the lateral resolutions achieved via structured illumination embedded speckle microscope is superior to what is achieved using the conventional arrangements. It can be observed that in comparison to conventional microscopy (600 ± 5 nm), SIM (390 ± 5 nm) improves the lateral resolution by ~ 35%. Further, structured illumination embedded speckle microscopy (310 ± 5 nm) improves the lateral resolution by ~ 20% and ~ 48% in comparison to SIM and conventional microscopy, respectively. Even though the results clearly show an improvement in lateral resolution using the proposed microscope, there isn't any observable difference in the lateral resolutions achieved using static and dynamic speckle patterns embedded within structured illumination. In order to elucidate further on the advantages of using static and dynamic aperiodic structures within the conventional SIM gratings, the image quality must also be assessed.

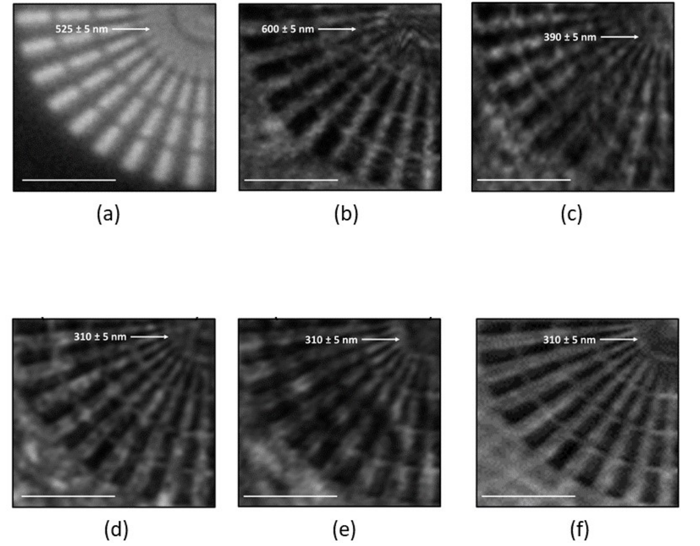

Fig. 11. Measurement of lateral resolution of the conventional systems including SEM, conventional microscopy and SIM using Siemen's star as the test sample is shown in (a), (b) and (c), respectively. The improved lateral resolutions measured by embedding static and dynamic speckle patterns within the conventional gratings are shown in (d), (e) and (f), respectively.

3.5 *Image Quality Metrics for the proposed configuration*

The image quality of the images captured using different configurations (for details, see section: *2.4*) is assessed using two parameters namely, mean square error and peak signal-to-noise ratio. The images captured have to be compared with the ground truth image to benchmark their quality. The image of the Siemen's star, which is used as the test sample obtained using SEM is used as a ground truth image since this image is closest to the actual Siemen's star pattern. The ground truth image captured using SEM is compared with the images captured using structured illumination embedded speckle microscopy and conventional optical configurations.

The MSE evaluates pixel-to-pixel variation between two images using Eq 2. Higher the MSE, more the variance of pixel values between the two Images. Here, we calculate the MSE values by comparing the image captured using the SEM to the image captured using the structured illumination embedded speckle microscope and the conventional microscope. The calculated MSE values are plotted in Figure 12.

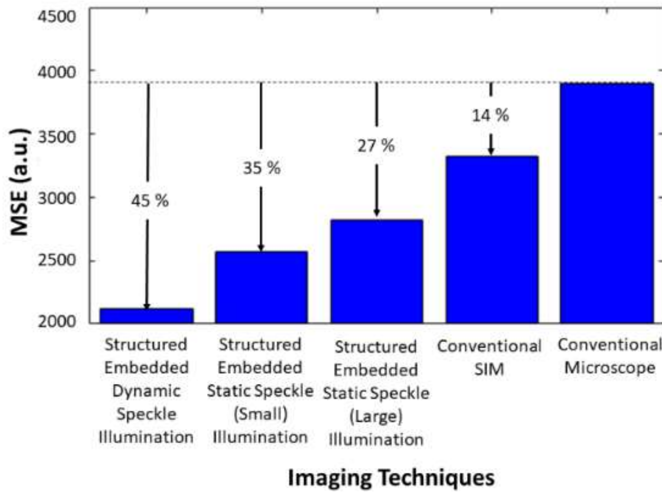

Fig. 12. Image quality metric calculation MSE calculated for the Siemen's star imaged using the conventional and the proposed techniques.

MSE of the image captured using the structured illumination embedded speckle microscope is substantially lower than the conventional methods. Further, the image captured using the structured embedded dynamic speckle illumination microscope shows the lowest MSE. In addition, compared to the conventional microscope, SIM enhances the imaging quality only by ~ 14%. In contrast to the conventional microscopic imaging, structured illumination embedded speckle microscopy employing large and small sized speckle patterns is observed to improve the MSE by ~ 27% and ~ 35%, respectively. Finally, structured illumination embedded speckle microscopy employing dynamic speckles improved the MSE by ~ 45% compared to the conventional microscope using the same microscope objective lens.

Since MSE compares the "true" pixel values of the two images, estimating the ratio between the maximum value of the signal to the maximum power of the distorting noise would be a more relevant metric [46]. PSNR is usually expressed using a decibel scale. The comparison of PSNR values are shown in Figure 13.

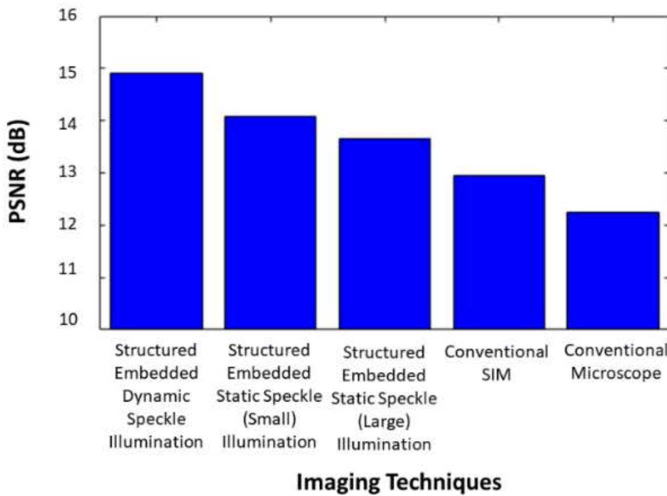

Fig. 13. Image quality metric calculation PSNR calculated for the Siemen's star imaged using the conventional and the proposed techniques.

From equation (3), MSE and PSNR are inverse proportional (for details, see section: *2.4*). Notably, lower the MSE value, higher the PSNR. Similar to the outcome of computing MSE, it can be observed that the PSNR value of structured illumination embedded speckle microscope is higher compared with conventional microscopy. Both MSE and PSNR analysis therefore confirm the improved imaging quality of the proposed configuration in comparison with the conventional techniques.

Even though structured illumination embedded speckle microscope shows improved imaging resolutions and quality, it is essential to understand the limitations of the system due to the sensitivity and switching speed of the imaging camera and LCOS-SLM, respectively. Improving the switching frequency and the use of a high speed sCMOS camera would improve the system performance for industrial applications that require high imaging resolutions and will form part of the future research direction in this area. Another future research direction would be to identify the opportunities and benefits provided by the proposed microscope in a transmission mode.

4. Conclusion

In this paper, we have developed a microscope using the combined advantages of structured illumination and embedded laser speckles. This concept and equipment which is named as structured illumination embedded speckle microscopy provides sub-diffraction limit resolution imaging with a high SNR. Since the projected speckle patterns act as pinholes (reducing the scattering noise), applying the conventional SIM algorithm further improves the imaging resolution and SNR. An imaging resolution of ~ 310 ± 5 nm (~ 48 % improvement in comparison with conventional microscopy) was achieved when viewed with a microscope objective (0.55 NA; 50X) having 11 mm long working distance using a Siemen's star as the test sample. In addition, the MSE was observed to be improved by ~45%.

Based on the study conducted, while the imaging resolution improvement was observed to be independent of the speckle size, the enhancement of SNR was observed to strongly dependent on it. It is envisaged that this demonstrated high-resolution, high SNR microscope can enable a paradigm shift in engineering applications.

Acknowledgements

We would like to acknowledge the fruitful discussions with Professor Nikolay Zheludev (University of Southampton) and his support. The idea of embedding speckles inside structured light pattern is initially conceived by S.M.P and extended along with discussions with V.M.M, AS and AH for the research presented in the paper. A.H, S.M.P and A.S performed experiments, image processing and analysed the data along with V.M.M. Custom Siemen's star target was designed and fabricated by O.B. V.M.M corrected and revised the manuscript contents prepared by AH. All authors gave suggestions, read and approved the final manuscript. V.M.M advised and supervised the research as principal investigator of the project. The research was performed when the authors S.M.P and A.S were research staffs attached to V.M.M at the Centre for Optical and Laser Engineering (COLE), Nanyang Technological University. The authors declare no competing financial interests. A.H‡ and S.M.P‡ contributed equally.

Funding

The authors acknowledge the financial support received through MOE (RG162/15 and RG192/17) and COLE-EDB.

References

1. Minsky, M., Memoir on inventing the confocal scanning microscope. Scanning, 1988. 10(4): p. 128-138.
2. Shinde, A., Perinchery, S. M., & Murukeshan, V. M. (2017). A targeted illumination optical fiber probe for high resolution fluorescence imaging and optical switching. Scientific reports, 7, 45654.
3. Wilson, T., Confocal Microscopy, in Microanalysis of Solids, B.G. Yacobi, D.B. Holt, and L.L. Kazmerski, Editors. 1994, Springer US: Boston, MA. p. 219-232.
4. Ganesha, U., et al., Characterization of surface topography by confocal microscopy: I. Principles and the measurement system. Measurement Science and Technology, 2000. 11(3): p. 305.
5. Mohankumar, V. K., Padmanabhan, P., Sathiyamoorthy, K., Murukeshan, V. M., Joseph, J., & Bhakoo, K. K. (2011). High resolution optical imaging of epithelial and neuronal cells. Journal of Medical Imaging and Health Informatics, 1(4), 354-359.
6. Yin, S., et al., Kinoform-based Nipkow disk for a confocal microscope. Applied Optics, 1995. 34(25): p. 5695-5698.
7. Perinchery, S. M., Shinde, A., Fu, C. Y., Hong, X. J. J., Baskaran, M., Aung, T., & Murukeshan, V. M. High resolution iridocorneal angle

imaging system by axicon lens assisted gonioscopy. Scientific Reports, (2016), 6, 30844.

8. Li, Q., Reinig, M., Kamiyama, D., Huang, B., Tao, X., Bardales, A., & Kubby, J. (2017). Woofer–tweeter adaptive optical structured illumination microscopy. Photonics Research, 5(4), 329-334.
9. Schulz, O., et al., Resolution doubling in fluorescence microscopy with confocal spinning-disk image scanning microscopy. Proceedings of the National Academy of Sciences, 2013. 110(52): p. 21000.
10. M.G.L. Gustafsson, Nonlinear structured-illumination microscopy: wide-field fluorescence imaging with theoretically unlimited resolution. Proceedings of the National Academy of Sciences of the United States of America 102, 13081-13086 (2005).
11. M.G.L. Gustafsson, Surpassing the lateral resolution limit by a factor of two using structured illumination microscopy. Journal of microscopy 198, 82-87 (2000).
12. Dan, D., B. Yao, and M. Lei, Structured illumination microscopy for super-resolution and optical sectioning. Chinese Science Bulletin, 2014. 59(12): p. 1291-1307.
13. Heintzmann, R. and T. Huser, Super-Resolution Structured Illumination Microscopy. Chemical Reviews, 2017. 117(23): p. 13890-13908.
14. S.W. Hell, J. Wichmann, Breaking the diffraction resolution limit by stimulated emission: stimulated-emission-depletion fluorescence microscopy. Optics letters 19, 780-782 (1994).
15. M.J. Rust, M. Bates, X. Zhuang, Sub-diffraction-limit imaging by stochastic optical reconstruction microscopy (STORM). Nature methods 3, 793-796 (2006).
16. H. Shroff, C.G. Galbraith, J.A. Galbraith, E. Betzig, Live-cell photoactivated localization microscopy of nanoscale adhesion dynamics. Nature methods 5, 417-423 (2008).
17. Yuan, G. H., Rogers, E. T., and Zheludev, N. I. Achromatic super-oscillatory lenses with sub-wavelength focusing. Light: Science & Applications, 6(9), e17036. (2017)
18. Rogers, K. S., Bourdakos, K. N., Yuan, G. H., Mahajan, S., & Rogers, E. T. Optimising superoscillatory spots for far-field super-resolution imaging. Optics express, 26(7), 8095-8112 (2018)
19. Roy, T., Rogers, E. T., Yuan, G., & Zheludev, N. I. Point spread function of the optical needle super-oscillatory lens. Applied Physics Letters, 104(23), 231109 (2014).
20. Yuan, G. H., Rogers, E. T., & Zheludev, N. I. Achromatic super-oscillatory lenses with sub-wavelength focusing Running title: Super-oscillatory achromatic lenses (2017).
21. Richard, L. and S. Ben, Applications of super-resolution imaging in the field of surface topography measurement. Surface Topography: Metrology and Properties, 2014. 2(2): p. 023001.
22. Vogel, M., et al. Structured-illumination microscopy on technical surfaces: 3D metrology with nanometer sensitivity. in SPIE Optical Metrology. 2011. SPIE.
23. Vogel, M., et al. Tuning structured illumination microscopy (SIM) for the inspection of micro optical components.
24. Kranitzky, C., et al. 3D-microscopy with large depth of field. in DGaO Proceedings. 2009.
25. Yang, Z., A. Bielke, and G. Häusler, Better three-dimensional inspection with structured illumination: speed. Applied Optics, 2016. 55(7): p. 1713-1719.
26. Yang, Z., A. Kessel, and G. Häusler, Better 3D inspection with structured illumination: signal formation and precision. Applied Optics, 2015. 54(22): p. 6652-6660.
27. Sandeep Menon Perinchery, Aswin Haridas, Anant Shinde, Oleksandr Buchnev, and Vadakke Matham Murukeshan, "Breaking diffraction limit of far-field imaging via structured illumination Bessel beam microscope (SIBM)," Opt. Express 27, 6068-6082 (2019).
28. García, Javier, Zeev Zalevsky, and Dror Fixler. "Synthetic aperture superresolution by speckle pattern projection." Optics express 13.16 (2005): 6073-6078.
29. Marom, Emanuel, Eyal Ben-Eliezer, and Naim Konforti. "Super-resolving-extended depth of field imaging system encoded by speckle pattern." Speckle06: Speckles, From Grains to Flowers. Vol. 6341. International Society for Optics and Photonics, 2006.
30. Fixler, Dror, et al. "Speckle random coding for 2D super resolving fluorescent microscopic imaging." Micron 38.2 (2007): 121-128.
31. Ben-Eliezer, Eyal, and Emanuel Marom. "Aberration-free superresolution imaging via binary speckle pattern encoding and processing." JOSA A 24.4 (2007): 1003-1010.
32. Mudry, Emeric, et al. "Structured illumination microscopy using unknown speckle patterns." Nature Photonics 6.5 (2012): 312-315.
33. Ben-Eliezer, Eyal, Naim Konforti, and Emanuel Marom. "Super resolution imaging with noise reduction and aberration elimination via random structured illumination and processing." Optics express 15.7 (2007): 3849-3863.
34. Idier, Jérôme, et al. "On the Superresolution Capacity of Imagers Using Unknown Speckle Illuminations." IEEE Transactions on Computational Imaging 4.1 (2018): 87-98.
35. Kim, MinKwan, et al. "Superresolution imaging with optical fluctuation using speckle patterns illumination." Scientific reports 5 (2015): 16525.
36. Yeh, Li-Hao, Lei Tian, and Laura Waller. "Structured illumination microscopy with unknown patterns and a statistical prior." Biomedical optics express 8.2 (2017): 695-711.
37. Jiang, S.-h. and J.G. Walker, Experimental confirmation of non-scanning fluorescence confocal microscopy using speckle illumination. Optics Communications, 2004. 238(1): p. 1-12.
38. Jiang, S.-h. and J.G. Walker, Non-scanning fluorescence confocal microscopy using speckle illumination and optical data processing. Optics Communications, 2005. 256(1): p. 35-45.
39. Shi-Hong, J. and G.W. John, Speckle-illuminated fluorescence confocal microscopy, using a digital micro-mirror device. Measurement Science and Technology, 2009. 20(6): p. 065501.
40. Jiang, S. and J. Walker, Differential high-speed digital micromirror device-based fluorescence speckle confocal microscopy. Applied Optics, 2010. 49(3): p. 497-504.
41. Ventalon, Cathie, and Jerome Mertz. "Dynamic speckle illumination microscopy with translated versus randomized speckle patterns." Optics Express 14.16 (2006): 7198-7209.
42. Lim, Daryl, et al. "Optically sectioned in vivo imaging with speckle illumination HiLo microscopy." Journal of biomedical optics 16.1 (2011): 016014.
43. Ventalon, Cathie, and Jerome Mertz. "Quasi-confocal fluorescence sectioning with dynamic speckle illumination." Optics letters 30.24 (2005): 3350-3352.
44. Rainer Heintzmann, Structured Illumination Methods. Handbook of Biological Confocal Microscopy, Springer, Boston, 265-279 (2006).
45. Shinde, A. B., Perinchery, S. M., & Matham, M. V. Fiber pixelated image database. Optical Engineering, 55(8), 083105 (2016).
46. Pappas, T. N., Safranek, R. J., & Chen, J., "Perceptual criteria for image quality evaluation. Handbook of image and video processing,"669-684 (2000).

Appendix A: Process Flowchart

Figure 14, shows the flowchart describing the modes of operation of the proposed system. For every image captured at x_1, y_1, z_1, the system offers two capabilities, namely, structured illumination and structured embedded speckle illumination. The former requires projection of periodic gratings (phases, φ_1, φ_2 and φ_3; angles, θ_1, θ_2 and θ_3) and the implementation of the conventional SIM algorithm. Alternatively, for the latter, the SIM algorithm is applied for every speckle pattern embedded (diffuser position D_1 to D_z) within the conventional structured illumination (phases, φ_1, φ_2 and φ_3; angles, θ_1, θ_2 and θ_3). For SIM, the resultant image I_p is calculated using the conventional algorithm. In contrast, for structured illumination embedded speckle microscope, the resultant image I_p' is estimated as an average of intermediate images calculated using the conventional SIM algorithm for different diffuser positions (Ip_{D1} to Ip_{Dz}). The process is then repeated for different sample depths positions, x_m, y_m, z_m.

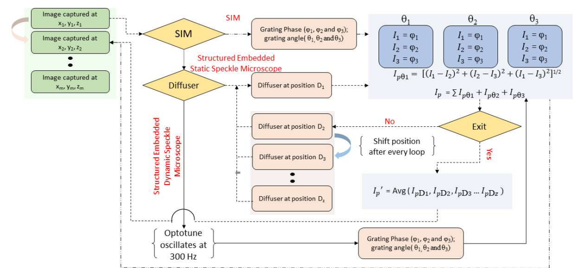

Fig. 14. Process flowchart for the proposed system. The flowchart describes the modes of operation of the system.

Appendix B: Spatial Resolution of a conventional microscope

Circular profile sections along the diameter of the Siemen's star image captured using the SEM is analyzed for reference. The normalized circular profile of a section (shown in Fig 15 (a)) along the diameter of

the Siemen’s star is shown in Fig 15 (b). The frequency spectrum of the circular profile is plotted in Fig 15 (c).

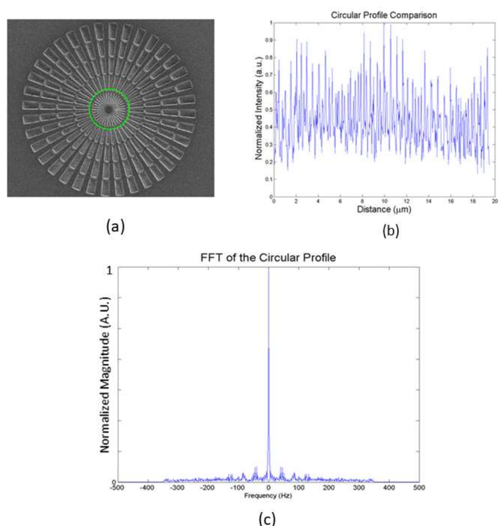

Fig.15. (a) SEM images using a Siemen’s star as the test sample. The profile of the circular section indicated by the green circle in (a) is shown in (b). The FFT of the circular profile is shown in (c). The white scale bar indicates 7.5 μm.

Figure 16, shows the comparison of circular section profiles of the Siemen’s star imaged using a conventional microscope and SIM. Notably, the presence of scattering noise in conventional microscopes and grid pattern noise in SIM hinders the spatial resolution.

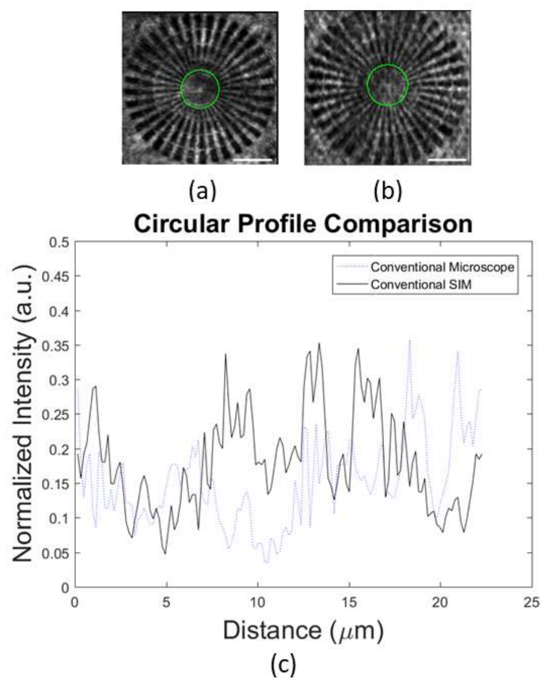

Fig.16. Images obtained from the conventional microscope and SIM using a Siemen’s star as the test sample is shown in (a) and (b), respectively. The comparison of circular section profiles of the Siemen’s star indicated by the green circles in (a) and (b) is